d-zero magnetism in nanoporous amorphous alumina membranes

Amir Sajad Esmaeily, M. Venkatesan, S. Sen, and J. M. D. Coey[*]
School of Physics and CRANN, Trinity College, Dublin 2, Ireland

Nanoporous alumina membranes produced by mild or hard anodization have a controllable pore surface area up to 400 times that of the membrane itself. They exhibit a temperature-independent and almost anhysteretic saturating response to a magnetic field up to temperatures of 300 K or more. The magnetism, which cannot be explained by the ∼1 ppm of transition-metal impurities present in the membranes, increases with the area of the open nanopores, reaching values of 0.6 Bohr magnetons per square nanometer for mild anodization and 8 Bohr magnetons per square nanometer for the faster hard anodization process. Crystallization of the membrane or treatment with salicylic acid can destroy 90% of the magnetism. The effect is therefore linked with the surfaces of the open pores in the amorphous Al_2O_3. Possible explanations in terms of electrons associated with oxygen vacancies (F or F^+ centers) are considered. It is concluded that the phenomenon involved is likely to be saturating giant orbital paramagnetism, rather than any sort of collective ferromagnetic spin order.

I. INTRODUCTION

d-zero magnetism is the ferromagneticlike response to an applied magnetic field of a material that is formally devoid of the unpaired 3*d* electrons usually needed for high-temperature magnetic order [1,2]. The effect is weak with little or no coercivity or temperature dependence of the magnetization curve—a typical order of magnitude of the saturation moment measured at room temperature is a Bohr magneton per square nanometer of surface. There is no generally accepted explanation. Doubts persist about the reality of the phenomenon because there are a number of well-documented artifacts and impurity effects [3–9] that might explain some of the measurements.

Many of the materials that display the effect are oxides. The effect is generally absent or undetectable in well-crystallized bulk material. It appears in polycrystalline granular solids [10], fine powders [11], thin films [12,13], single-crystal surfaces [11,14], and nanoparticles [15–19]. CeO_2 is the example that has been most intensively studied [20]. Much evidence suggests that *d*-zero magnetism is a surface or interface phenomenon, which is why the magnitude of the saturation moment is often quoted per unit surface area. There are about 18 surface oxygen ions per square nanometer at a close-packed oxygen surface, but surfaces, especially in ambient conditions, are difficult to characterize because they tend to reconstruct and attract adlayers of water. Experience with oxide interfaces, which are liable to exhibit emergent properties such as metallic conduction or magnetism that are absent from either of the constituents, alerts us to the possibility of a different electronic state at the surface or interface. A famous example is the $LaAlO_3$/$SrTiO_3$ interface [21–23], which can be metallic or magnetic although neither oxide by itself has these properties in the bulk. (Irradiated $SrTiO_3$ crystals [24] and the surface of $SrTiO_3$ crystals [11] have recently been shown to exhibit features typical of *d*-zero magnetism.) Some form of reconstruction, whether by charge transfer or atomic rearrangement, often in the form of oxygen vacancies, is inevitable at an extended polar surface or interface in order to eliminate a divergence in energy known as the polar catastrophe that is associated with the electric field created by a sheet of surface charge.

Nanoporous oxide membranes are very interesting in this respect. The ratio ρ of internal surface area of the pores to the area of the two flat surfaces of a membrane of thickness t_m with a regular hexagonal array of pores of radius r and spacing d is

$$\rho = 2\pi r t_m / \sqrt{3} d^2. \qquad (1)$$

For example, this ratio in a membrane with $d = 140$ nm, $r = 30$ nm, and $t_m = 40\,\mu$m exceeds 200. Such membranes thicker than 90 nm have most of their surface area in the pores. Micrometer-thick membranes therefore provide an excellent opportunity to enhance the surface/volume ratio in order to study surface magnetism in oxides. To achieve the same enhancement by reducing a crystal of the same thickness t_m to powder particles of radius r_p requires

$$\rho = 3t_m / 2r_p, \qquad (2)$$

or $r_p \approx 290$ nm for $t_m = 40\,\mu$m. It is relatively straightforward to produce a nanoporous oxide membrane electrochemically, but difficult to obtain a 600-nm ceramic powder by milling, although there are options to synthesize nanoparticles directly.

A few reports exist in the literature on the magnetism of nanoporous Al_2O_3 [25], TiO_2 [26], and Cu_2O [27], and Cu_2O/porous anodic alumina [28] films. Most remarkable is the report of Sun *et al.* [25], who produced nanoporous alumina membranes of submicrometer thickness by brief mild anodization at 45 V in oxalic acid. These membranes exhibited ferromagneticlike signals in superconducting quantum interference device (SQUID) magnetometry that were as high as $60\,kAm^{-1}$ when the magnetic field was applied perpendicular to the plane of the membrane, but there was a linear, paramagnetic

[*]Corresponding author: jcoey@tcd.ie

TABLE I. Characteristics of the third set of anodic alumina membranes.

Anodization voltage (V)	Type	Thickness (μm)	Magnetic moment (Am^2)	Pore size (nm)	Interpore distance (nm)	ρ
20	Mild	3.32	6.2×10^{-9}	30	55	59.7
30	Mild	7.7	7.3×10^{-9}	41	80	89.4
50	Mild	27.3	1.7×10^{-8}	69	120	237.2
110	Hard	31.4	3.8×10^{-8}	57	260	48.0
120	Hard	35.4	4.2×10^{-8}	60	285	47.0
130	Hard	40.1	4.4×10^{-8}	62	310	46.9

response when the field was applied in-plane (For comparison, the magnetization of Ni is 500 kAm^{-1}.)

Here we have conducted a systematic investigation of the magnetic properties of nanoporous amorphous alumina membranes prepared by a mild, two-step [29] or hard, single-step [30] anodization process. We find magnetic signals that are an order of magnitude or more greater than anything that could be explained by 3d impurities that are present at a level of less than 1 ppm in our samples. The magnetism is associated with the pore surfaces. We discuss possible explanations of its origin and sign.

II. EXPERIMENTAL METHODS AND MATERIALS

The aluminum foil used for anodization was supplied by Advent Research Materials (UK). It is 250 μm thick and nominally 5N (99.999%) pure with stated impurity levels of ferromagnetic elements Fe $<$ 0.7 ppm and Ni $<$ 0.6 ppm. 12-mm disks were cut with a steel punch, and the disks were mounted in a Teflon cell where the central 7 mm of the disk forming the anode in an electrolytic cell was exposed to the electrolyte and electropolished.

Four sets of samples were prepared by the mild two-step method in 0.3 M oxalic acid at 17 °C at voltages ranging from 5 to 70 V. A first step of anodization was carried out at the selected voltage for 5 h. The disordered oxide layer so formed was then removed using a solution containing 0.2 M chromic acid and 0.5 M phosphoric acid at 60 °C for 3 h. The exposed dimpled aluminum surface with regular or irregular dimples, depending on the applied voltage, was then reanodized in the mild second-step for a further 3 h at the selected voltage [29]. The hexagonal pore arrays could have a regular (30–50 V) or irregular (5–20 V and 60–70 V) structure. They are most regular for voltages around 40 V.

In addition, four sets of hard-anodized samples were prepared in a single-step process. They were started at 40 V for 10 min at 0 °C, and then continued into the hard regime by ramping up the potential at 30 V/min to a selected value in the range 80–140 V, where it was held for 20 min [30]. Argon was bubbled through the electrolyte during anodization of the third set, and extra voltage points were included in the fourth set. Anodization rates are an order of magnitude faster in the hard regime. Table I shows structural and magnetic properties of typical mild or hard anodized samples.

Another two sets of thinner, mild-anodized samples were prepared at 40 V with the same first step but varying the second-step anodization time from 2 to 60 min at 5 °C in order to have two sets of four very thin samples with different t_m, prepared in the same conditions as Ref. [25].

Small specimens (1 mm^2) used for analysis in a Zeiss Ultra scanning electron microscope (SEM) were cut with Ti scissors and coated with 2–5 nm of gold. Membrane thickness was determined by direct SEM observation of a fractured alumina surface at a kink in the membrane.

X-ray diffraction was performed on larger 20-mm disks, which were prepared in another cell. Photoluminescence (PL) was measured on one complete series of 7-mm-diameter membranes using 405-nm excimer laser excitation and on several larger disks. Selected samples, anodized at 20, 70, and 140 V were measured by electron paramagnetic resonance (EPR).

The specimens used for magnetic analysis were squares roughly 5 $\times$ 5 mm^2 cut from the centers of the disks with titanium scissors. When following this protocol, these samples were shown to be free of contamination by the iron that is introduced around the rim of the disk from the steel punch. The samples were mounted in straws for measurement in a 5-T Quantum Design SQUID magnetometer. After cutting, the samples were handled with tools made of wood or plastic.

All 12 samples in the second set were analyzed for traces of Mn, Fe, Co, and Ni using laser-ablated inductively coupled mass spectroscopy (LA-ICPMS).

III. EXPERIMENTAL RESULTS

Images of the membranes grown in the mild and hard regimes at different voltages are presented in Fig. 1. Pores increase in size with voltage, and their positions are irregular for voltages below 30 V. The arrays becomes periodic at 30–50 V and are most ordered at 40 V, but large $\sim$100-nm irregular pores appear in the mild regime above 50 V. Pores in the hard regime are about 50 nm in diameter, and more widely spaced with less dependence on the anodic voltage. Figure 2 shows plots of pore diameter 2r, average pore spacing d, and membrane thickness t_m as a function of voltage, covering both regimes. Unlike the mild case, the underlying pore structure in the hard case was not visible from the top surface of the one-step hard-anodized samples, so these had to be imaged from the bottom side. The aluminum substrate was chemically etched away using a solution comprising equal amounts of saturated CuSO$_4$ and HCl, and the alumina barrier layer was then removed by argon ion milling to expose the pores. The structures of the mild and hard membranes are illustrated schematically by insets in Fig. 2(a). Pore spacing depends only on voltage at the metal/electrolyte interface, but pore diameter and membrane thickness also depend on temperature and the product of growth rate and time, respectively.
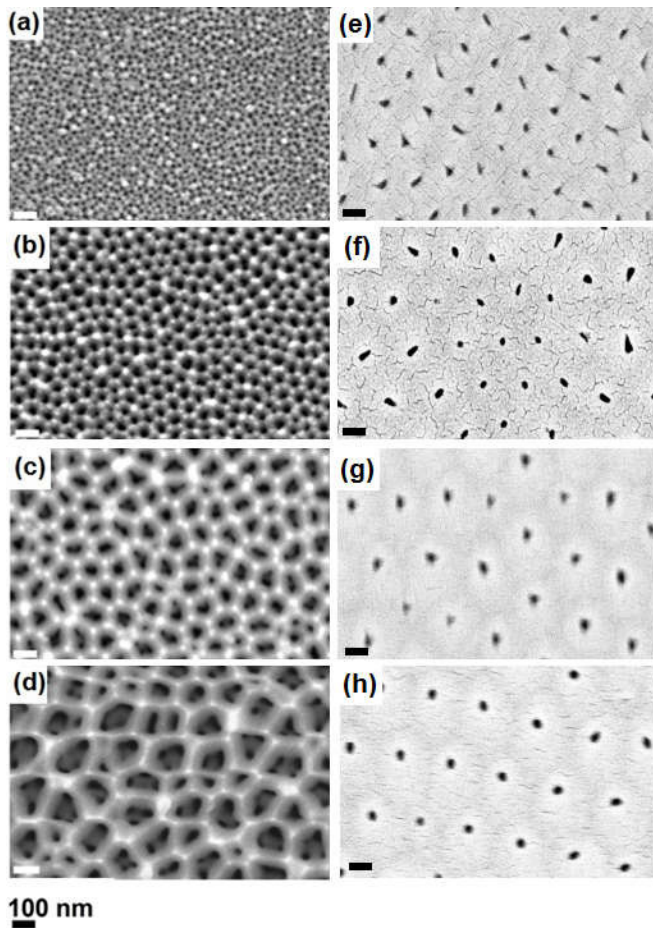
FIG. 1. Evolution of pore structure with anodization voltage. The left column is for mild anodization at 17 °C (10, 30, 50, 70 V); the right column is for hard anodization at 0 °C (80, 100, 120, 140 V). Scale bars are 100 nm. Details of sample preparation are described in the text.
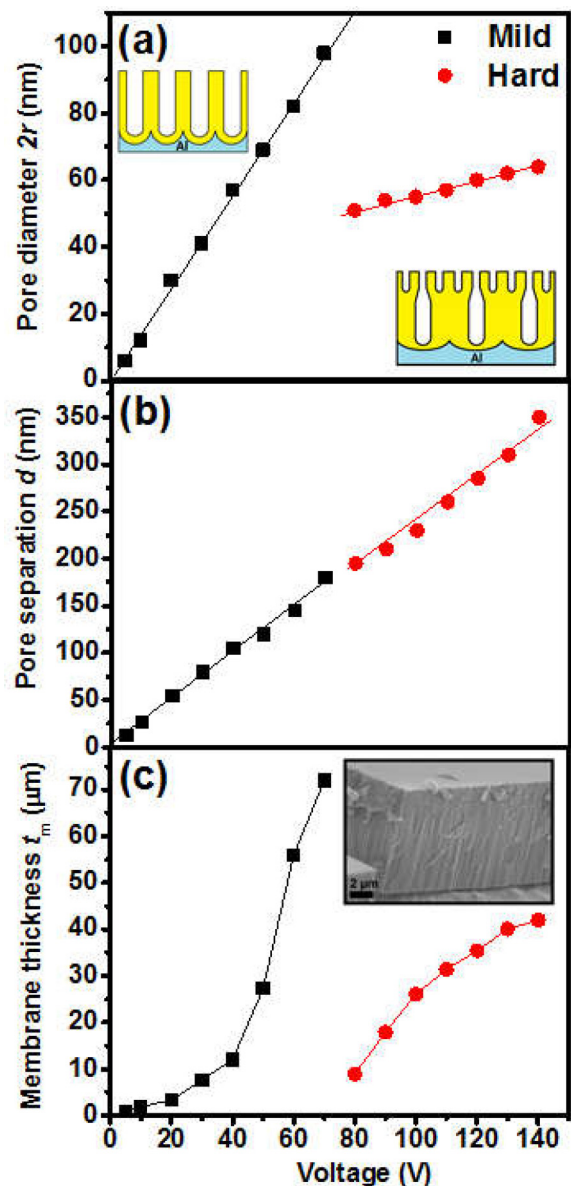

FIG. 2. Plots of (a) average pore diameter (insets indicate the structures of soft- and hard-anodized membranes), (b) average interpore distance, and (c) membrane thickness as a function of voltage, spanning the mild and hard anodization regimes. The inset in (c) shows the cross section of a typical membrane fracture surface (80 V) used for thickness measurements.

X-ray diffraction patterns of both types of membranes after removing the Al substrate are illustrated in Fig. 3. They are amorphous, but crystallize in the cubic γ-Al_2O_3 structure when heated to 1000 °C in a vacuum of 10^{-7} mbar. Density measurements on mild- and hard-anodized membranes yield values of 2054 and 2291 kg m^{-3} (including the pores), respectively. Comparison with the value of 3300 kg m^{-3} for random dense-packed amorphous alumina [31] indicates that the membranes have a significant free volume, in addition to their open porosity. The free volume contributes to the remarkable plasticity of this material, which aids the formation of the regular arrays of nanopores [32].

Photoluminescence spectra (Fig. 4) exhibit a peak at 520 nm, which tends to increase in intensity with membrane thickness in the mild and hard regimes, and the intensity is also found to increase monotonically with interpore spacing [Fig. 4(b)].

The magnetization curve of the unoxidized aluminum illustrated in Fig. 5(a) shows a paramagnetic mass susceptibility of $\chi_m(Al) = 7.3 \times 10^{-9}$ m^3 kg^{-1}, in agreement with the literature value of 7.6×10^{-9} m^3 kg^{-1}. This susceptibility increases by 12% on cooling from 300 to 4 K, but there

is no sign of any paramagnetic Curie law upturn associated with isolated paramagnetic ions in the metal foil. Isolated Fe atoms in Al are nonmagnetic, with a Kondo temperature on the order of 5000 K [33]. The linear susceptibility of the foil is superposed on a very small saturating magnetic moment of about 1.6×10^{-9} Am^2, shown in the inset, which corresponds to 0.33 ppm of ferromagnetic iron impurity, an amount that is compatible with the nominal ($<$0.7 ppm) iron content of the foil. LA-ICPMS measurements of the iron content of 12 membranes oxidized at voltages ranging from 20 to 130 V show values averaging to 0.45 ± 0.15 ppm, with no systematic dependence on voltage. The average content of Mn, Co, and Ni is even smaller, 0.02(3) ppm, 0.01(2)ppm, and 0.05(6) ppm,
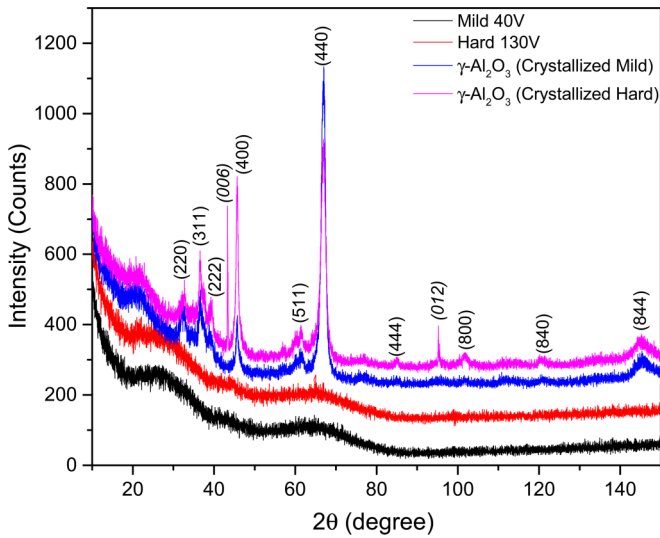
FIG. 3. X-ray diffraction patterns of amorphous alumina membranes produced at 70 and 130 V. The pattern after heating at 1000 °C in vacuum for 120 min shows crystallization of the membrane into γ-Al_2O_3. The four data sets are offset by 50 counts for clarity. α-Al_2O_3 peaks are indexed in italics.

respectively. All magnetic moments quoted here in Am^2 are normalized to a sample area of 25 mm^2.

Magnetization curves for two extreme samples, one a thin membrane anodized at 10 V and the other a thick membrane anodized at 140 V, are shown in Figs. 5(c) and 5(d), respectively. The data are corrected for the paramagnetism of the aluminum substrate ($\chi = 19.6 \times 10^{-6}$), which gives a contribution of about 200×10^{-9} Am^2 in 2 T, and the diamagnetic contribution of the alumina itself ($\chi = -19.1 \times 10^{-6}$). There remains the weak "ferromagneticlike" moment of interest to us here, as well as a paramagnetic Curie-law contribution at low temperatures. Figures 5(a) and 5(c), inset, show the same slope, but the temperature-dependent scan of the moment of a membrane on its Al substrate in fixed field in Fig. 5(b) shows a Curie-law upturn at low temperature, superposed on an almost constant temperature-independent saturated ferromagneticlike signal and the net paramagnetic background from aluminum and alumina. The Curie-law term would correspond to the presence of about 0.1 ppm of paramagnetic Fe^{3+} in the alumina, or 1.2 ppm of free spins.

Generally the magnetic signals from the anodized membranes after correction for the susceptibility of the underlying unanodized aluminum exhibit a ferromagneticlike response
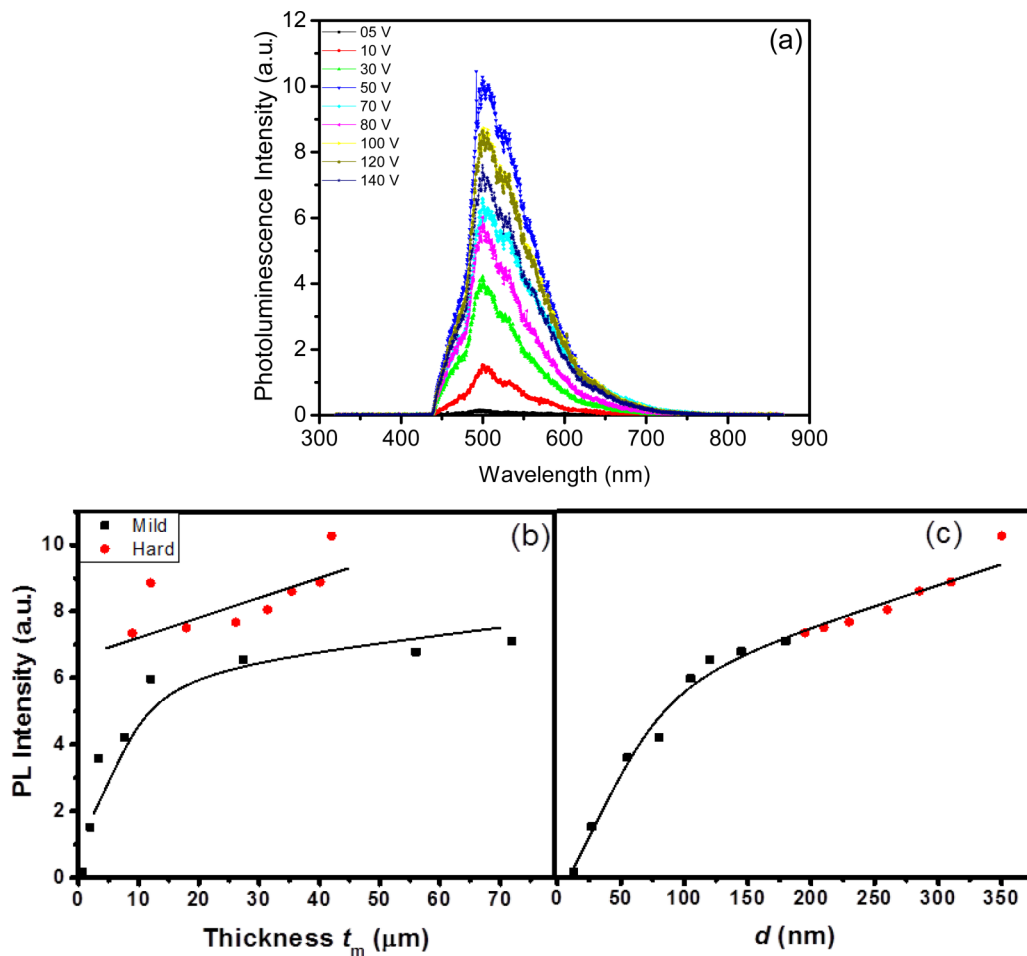

FIG. 4. (a) Photoluminescence spectra of the fourth set of amorphous alumina membranes prepared at different anodization voltages with an excitation wavelength of 405 nm, and the line intensity plotted as a function of membrane thickness (b) and interpore spacing (c). The solid lines are guides to the eye.
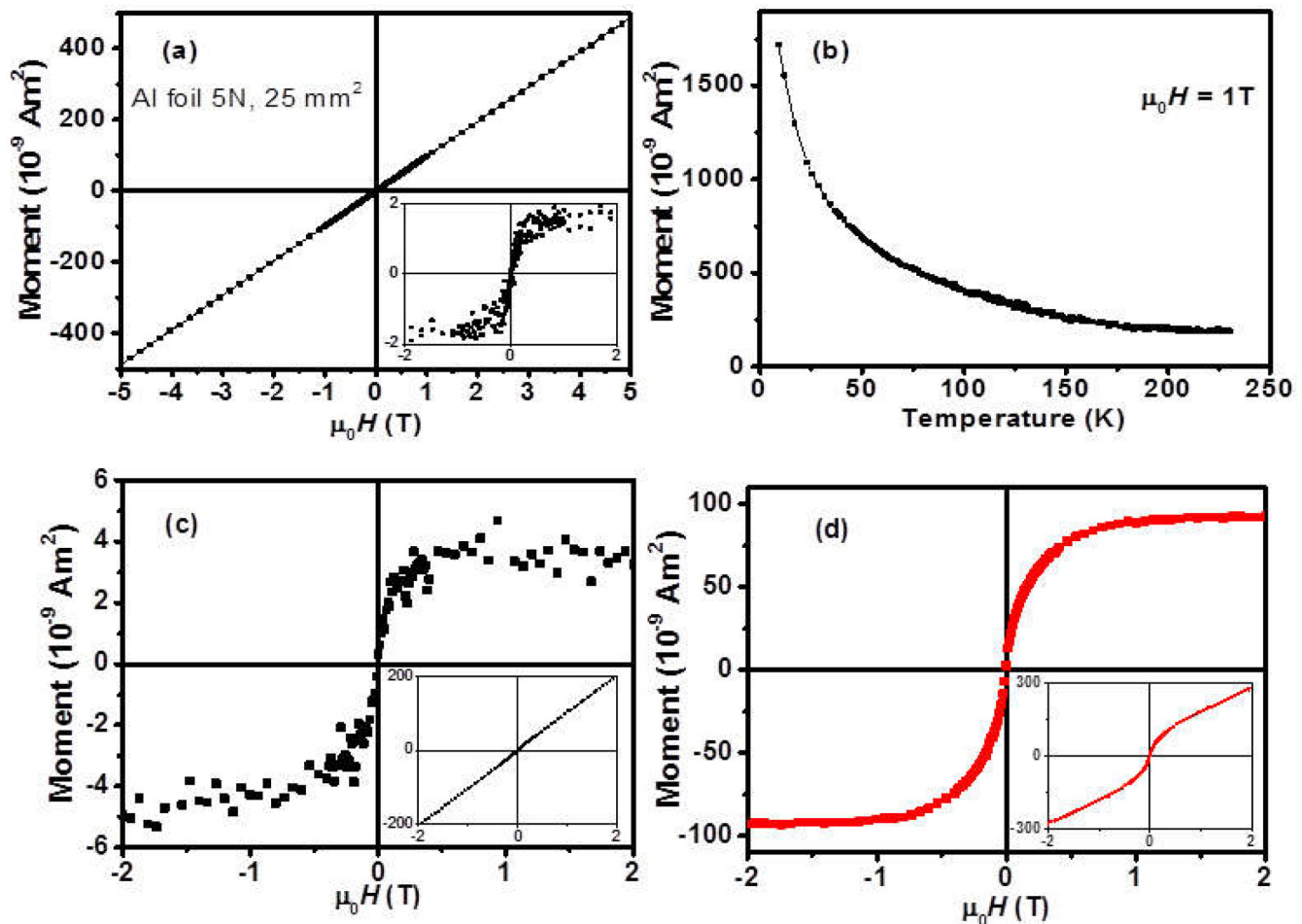
FIG. 5. Magnetization curves for aluminum and for two alumina membranes. All moments shown are for 5×5-mm^2 samples. (a) Moment of the aluminum foil on which the membranes are grown; (Inset) small residual signal after correction for the paramagnetic susceptibility, corresponding to 0.3 ppm of ferromagnetic impurity; (b) thermal scan of the moment in 1 T for an aluminum foil anodized at 70 V. Room-temperature magnetization curves for a mild- (10 V) (c) and hard-anodized membranes (140 V) (d) from set 4. The data are corrected for the net paramagnetic slope; uncorrected data are shown in the insets.

to the applied magnetic field, which saturates in a field of approximately 0.5 T. The signal is 3–60 times greater than anything that could be ascribed to ferromagnetic contamination by metallic iron of the aluminum or the membrane itself.

Further examples for a mild-anodized and a hard-anodized membrane are shown in Fig. 6, where the magnetization curves measured at 300 and 4 K are compared. The observed coercivity is minimal, <5 mT at both temperatures, and effectively zero within the error expected after saturating the magnetization in 5 T. The values measured after magnetizing in 1 T are again <5 mT. Just as remarkable is the absence of any temperature dependence of the ferromagneticlike magnetization curve of these samples between 300 and 4 K. Furthermore, the magnetization curve is practically identical for these membranes, regardless of whether the field is applied parallel or perpendicular to the membrane surface [Fig. 6(c)]. For another membrane, where superposing magnetization curves were measured at four temperatures between 400 and 4 K, the saturation magnetization differed by no more than 3%, which would imply a Curie temperature of more than 1000 K, assuming a temperature dependence given by Bril-

louin theory for $S = 1$. The data on this mild-anodized sample are presented in Fig. 7, where the superposed magnetization curves are shown in (a), and the temperature (in)dependence of the magnetization measured in fixed fields is shown in (b).

For the two extra series of thin ($t < \sim 1$ μm), 40-V membranes mild-anodized at 5 °C, the moments are proportionately smaller than for the thick membranes, and no anisotropy of the magnetization curves was found when the field was applied perpendicular or parallel to the surface.

A summary of magnetic moment data for the four sets of membranes, normalized to a common area of 25 mm^2, is plotted on a log scale as a function of anodization voltage and porosity ratio in Fig. 8. For both hard- and mild-anodized membranes there is a tendency for the moment to increase with anodization voltage and membrane thickness. Although the values are rather scattered, the form of magnetization curve remains the same. In the plot of moment versus porosity in Fig. 8(b) the hard-anodized membranes are much more magnetic in relation to their porosity, reflecting their faster growth.
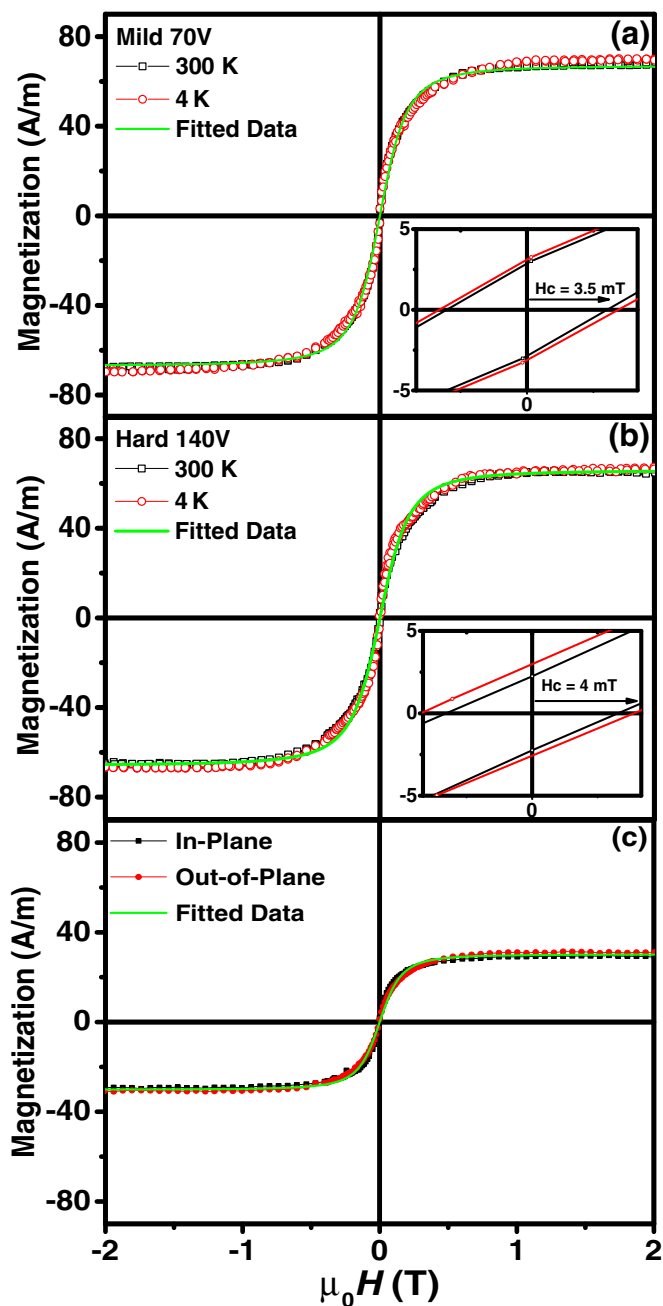
FIG. 6. Comparison of magnetization curves at 300 and 4 K for high-moment specimens anodized at (a) 70 and (b) 140 V. (c) Comparison of magnetization curves measured with the field, applied parallel and perpendicular to the surfaces of relatively thick membranes anodized at 50 V. The solid green curve is the fit to the theoretical function $M = M_s\, x/\sqrt{(1 + x^2)}$, where $x = C\mu_0 H$.
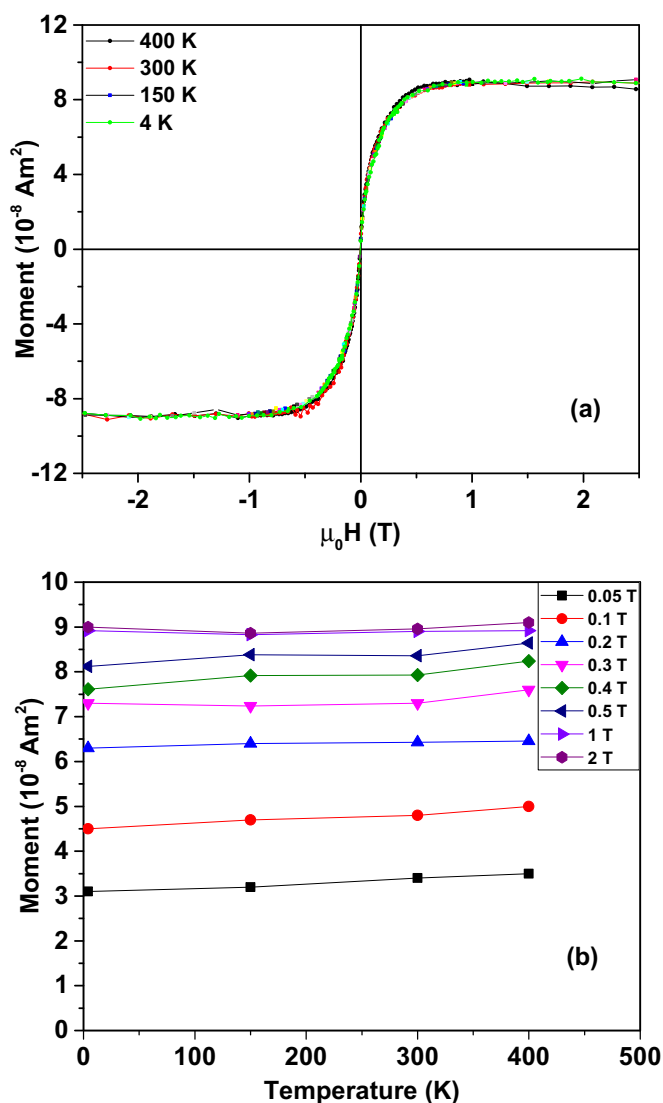

FIG. 7. (a) Superposition of magnetization curves of a mild-anodized membrane. (b) Magnetic moment plotted versus applied field at fixed fields, showing the absence of temperature dependence between 4 and 400 K.

The effect of crystallizing the amorphous alumina is illustrated in Figs. 9(a) and 9(b). Much of the porosity is eliminated, and the magnetic moment is largely destroyed by this treatment. A series of experiments that involved subjecting a 60-V membrane to a sequence of soaking in water or alcohol followed by vacuum treatment (Fig. 10) led to smaller changes of magnetic moment, with maximum reductions ranging from 10 to 80%. Most effective, however, is immersion of the membrane in a 1-M aqueous solution of salicylic acid ($C_7H_6O_3$) for 1 h, which has the effect of reducing the moment by 60–90% [Fig. 9(c)]. Salicylic acid is a catechol, recognized as having a strong affinity to aluminum oxide surfaces [34]. All these experiments provide good evidence of a surface origin of the magnetism. Buried impurities or secondary magnetic oxide phases with a high Curie temperature would be insensitive to such treatment.
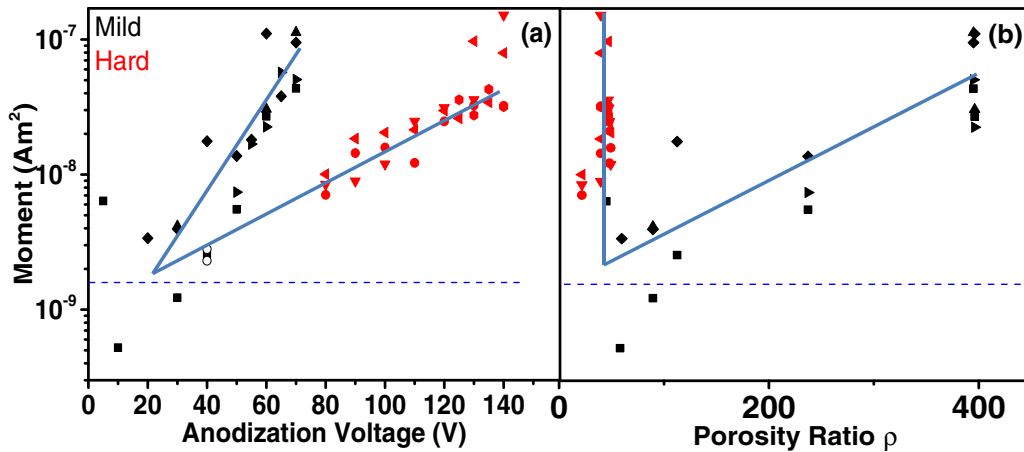

Salicylic acid
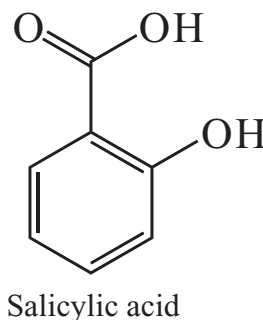
FIG. 8. (a) Compendium of magnetic moment data for the four sets of samples (solid symbols). (b) Plot of magnetic moment on a logarithmic scale as a function of porosity ratio for mild- (black) and hard- (red) anodized samples. The horizontal dashed line marks the moment due to iron contamination of the aluminum. The open circles in (a) are for membranes anodized at 40 V for an hour. Solid lines are guides to the eye.

The magnetic moment obtained from an amorphous alumina membrane is reduced by about 30% after annealing in argon at 500 °C for 6 h. The argon annealing intensifies the PL spectrum by factor of 3 [35].

Electron paramagnetic resonance spectra were measured for three of the membranes, anodized at 20, 70, and 140 V and freed from their aluminum substrates. Narrow absorption lines with a linewidth of 1.5 mT and $g = 2.003\,96$ are observed for the three specimens, changing little with the orientation of applied field relative to the membrane. The numbers of free spins per kg for the three specimens were estimated from the peak areas as 2.5×10^{19}, 4.6×10^{20}, and 7.4×10^{20}, respectively.

Finally, Fig. 11 shows the UV-vis spectra (transmission and absorption) for the third set of samples. New optical absorption appears and the band gap decreases from about 5.6 to 3.5 eV on increasing the anodization voltage from the mild to the hard regime.

IV. DISCUSSION

The data on these nanoporous structures establish the reality of *d*-zero magnetism in amorphous alumina, and allow us to characterize the phenomenon better than was possible previously. The LA-ICPMS analysis of 3*d* impurities in the membranes mentioned in Sec. III showed no trend with anodization voltage, and the measured moments are one or two orders of magnitude greater than could be accounted for by ferromagnetic metal impurities, as we see in Figs. 5 and 8.

The first question is, "Where in these membranes does the magnetism reside?" Since there is no such effect in well-crystallized alumina (sapphire) [36], and crystallization of the membranes tends to destroy the magnetic response [Fig. 9(b)], an origin connected with defects is clearly indicated. Anodic alumina has a highly defective amorphous structure with an internal free volume of 10–20%, in addition to the volume of the open nanopores. This was inferred by comparing the density extrapolated to zero open porosity (2945 kg m^{-3} for mild anodization or 2570 kg m^{-3} for hard anodization in oxalic acid [37] with that obtained on model amorphous structures (3300 kg m^{-3}) [31]. Our measured densities are comparable.

A defect origin has been adduced for similar magnetic responses in oxide single crystals [8,11], powders [15], thin films [38], and granular ceramics [5,39–41] both in the undoped and doped states [2]. The random coordination structure of amorphous alumina that includes 4-, 5-, and 6-coordinated Al, and a mixture of O^{2-} and OH^- ions is a potential store of dangling bonds. However, the ability of solvents and drying treatments to modify the magnetism quite significantly, Fig. 10, was the clue that we should be looking for surface defects at the open pores rather than internal defects in closed pores. The salicylic acid treatment [Fig. 9(b)], which adds coordinating ligands to surface aluminum ions [34], is a convincing confirmation that the origin of the magnetism must lie at the surfaces of the open pores in the membranes.

There is little atomic-scale experimental information on surface defects in amorphous alumina [42], but indirect information on the defects in the bulk is inferred from EPR or photoluminescence data. Calculations of the electronic structure of oxygen defects indicate that associated electronic states in the band gap may form conductive paths, which are thought to contribute to resistive switching [43]. In crystalline CeO_2, the oxygen vacancies form short linear chains on clean (111) surfaces that could constitute conducting paths [44].

Next, we evaluate the magnitude of the moment per unit pore surface area. The largest moment, observed in a 25-mm^2 140-V hard-anodized membrane with $t = 41\,\mu$m, $d = 330$ nm, and $r = 30$ nm, is 1.5×10^{-7} Am^2 (Fig. 8). From (1) we deduce $\rho = 41$, and a moment density of 8 μ_B nm^{-2}. The largest moment in the mild-anodized membranes is 1.1×10^{-7} Am^2 for a 70-V membrane with $t = 71\,\mu$m, $d = 175$ nm, and $r = 50$ nm, corresponding to $\rho = 398$, and a moment 0.6 μ_B nm^{-2}. The surface moment densities are therefore much greater for the more rapid, hard-anodized membranes, which is consistent with their lower density. Moment densities are similar to those found for the anhysteretic, temperature-independent surface magnetism of $SrTiO_3$ [11], due to localized or itinerant electrons associated with defect states at the pore surfaces. Oxygen vacancies are likely defects. It is widely believed that *F* centers (oxygen defects with two trapped electrons) and F^+ centers (oxygen defects with one trapped
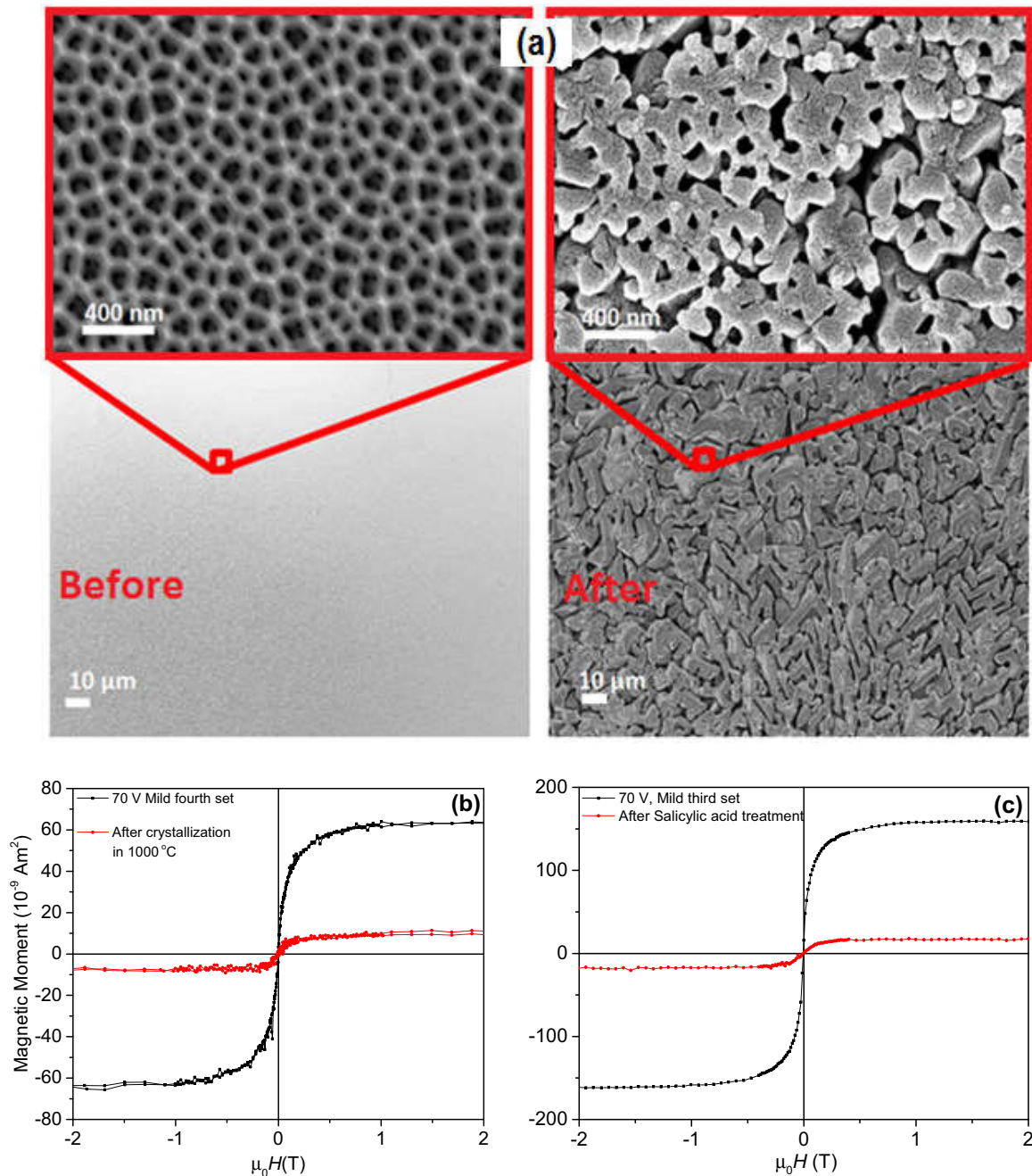
FIG. 9. Structure (a) of a 70-V mild-anodized membrane before and after crystallization at 1000 °C. The panel at the bottom left (b) shows the magnetization reduction on crystallization; the panel at the bottom right (c) shows a similar drastic reduction of the magnetization produced by treatment of the membrane in salicylic acid.

electron) are responsible for the photoluminescence spectra [35,42,45–51], and the EPR spectra have been attributed to F^+ centers [42,46] since the two electrons in an F center are expected to be spin paired. Table II summarizes the unpaired spin densities deduced from our EPR measurements, compared with the unpaired spin densities that would be needed to explain the saturating moments. The densities quoted are the number of unpaired spins per million Al atoms. The number of unpaired spins in EPR, or those deduced from the Curie-law upturn in susceptibility and those needed to account for the saturating moments, are quite different in magnitude, and

indeed there is no reason to expect them to be related. If there is ordered spin magnetization in the membranes, it will not give a sharp EPR signal, but rather a broad ferromagnetic resonance. Nor would it be expected to give a PL signal. A demonstration that the PL response and the d-zero magnetism are essentially unrelated was provided by heating the membranes to 500 °C in argon. This is known to enhance the PL signal by a factor of 3 [35], but there was no corresponding increase in magnetic moment; it decreased instead by 30%. We are dealing with two separate and independent electronic systems.
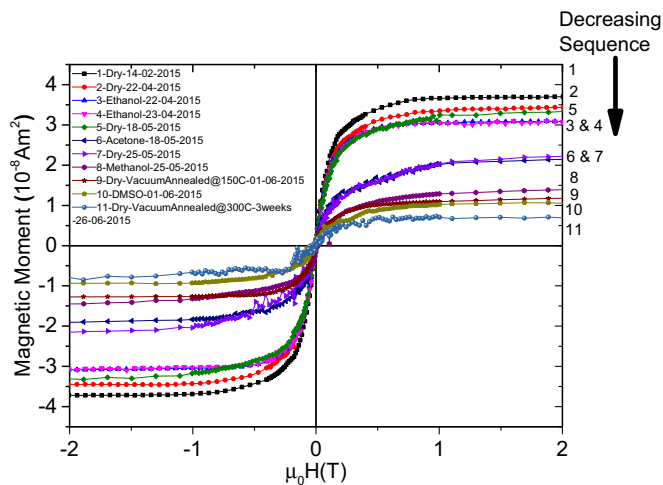
FIG. 10. Influence of a sequence of soaking and drying treatments with various solvents on the magnetic moment of a 60-V mild-anodized membrane.

The nonlinear, saturating magnetic signals associated with *d*-zero oxide surfaces or thin films are frequently assumed to be evidence of ferromagnetism, and therefore potentially interesting for spintronics [1]. This assumption is probably unwarranted. It is generally impossible to establish the existence of a reversible ferromagnetic-paramagnetic Curie temperature in these systems. To explain the observed temperature independence of the magnetization curves in terms of spin-based ferromagnetism would require a Curie temperature at the pore surface on the order of 1000 K, judging from the absence of temperature dependence of the magnetization below 300 K. To the best of our knowledge, there is no example in the literature of any material with itinerant or localized electrons having $s = 1/2$ that exhibits ferromagnetism at even one-tenth of this temperature.

The absence of magnetocrystalline anisotropy is understandable in an $s = 1/2$ system, but shape anisotropy would be expected if ferromagnetism were confined to a thin volume at the surface. For example, the maximum observed moment of $8 \, \mu_B \, nm^{-2}$ can be formally associated with a surface current around a pore of radius $r = 30 \, nm$, corresponding to an average magnetization of $(2/r)\sigma_m = 4.9 \, kAm^{-1}$, where σ_m is the surface moment density in A. It follows that the saturation of the magnetization in a field perpendicular to the plane should saturate practically immediately, but a field of $2.5 \, kAm^{-1}$ (3 mT) is needed in an in-plane direction, where the demagnetizing factor is $N = 1/2$. Dipolar interactions between neighboring cylinders will reduce the predicted anisotropy. Such a small difference in slope of the initial magnetization curves could not be detected in our measurements.

It is important to emphasize that the membranes are not superparamagnetic. Certainly, superparamagnets exhibit no hysteresis and saturate in relatively low magnetic fields, but their magnetization curves follow a Langevin function, and scale as (*H*/*T*) [33]. The initial slope in an external field should increase as $1/T$ until it is limited by the demagnetizing field. In the alumina membranes there is no temperature dependence at all, and no sign of blocking down to 4 K.

Magnetically ordered clusters of electron spins localized at oxygen vacancies, for example, would have been expected to behave superparamagnetically.

A further indication that the magnetic response may not be associated with a collectively ordered magnetic state of the spins of electrons associated with surface defects on the pore surfaces comes from the EPR spectra. The spin density estimated from the intensity of the narrow EPR line (width 1.5 mT) measured on a 70-V membrane is $0.94 \times 10^{24} \, m^{-3}$. These electrons are paramagnetic, not ferromagnetically ordered.

Since we cannot explain the temperature-independent, anhysteretic, defect-related d^0 magnetism in our membranes in terms of conventional ferromagnetism of exchange-coupled electron spins, we need a different explanation. Our idea is that we are seeing a type of saturating paramagnetism that is entirely field-induced and originates not from spin, but from orbital charge currents in mesoscopic coherent electronic domains that form in response to the zero-point fluctuations of the vacuum electromagnetic field. It was shown in Ref. [52] that such a stable coherent state was possible in theory for quasi-two-dimensional systems with a large surface-to-volume ratio. Treating the defects as simple electronic two-level systems with energy splitting $\hbar\omega$ captures the mixing of states required to produce a coherent thermally stable mesoscopic structure. The zero-point electromagnetic field of frequency ω mixes ground- and excited electronic states to create a coherent many-electron ground state which is stabilized by an energy $-G^2\hbar\omega$ per electron, where $G \sim 0.1$. The ground-state wave function of the many-electron coherent state does not have a well-defined angular momentum, as it is based on the sum of two states with different energy and angular momentum values [19], but an applied magnetic field stabilizes a particular orbital state. In the present case, the range of ω can be determined by cavity modes in the pores of length t_m where the relevant electrons are located. Allowed modes have frequency $\omega_n = 2\pi nc/t_m$, with a low-frequency cutoff at a wavelength $\lambda = t_m$.

The existence of a range of chemical effects of the zero-point fluctuations on material confined in various cavities has been demonstrated over the past few years by Ebbesen and co-workers [53–58], and he has recently summarized their results [58]. We think we are seeing a magnetic manifestation of this phenomenon in our nanoporous amorphous alumina.

Saturating orbital paramagnetism has previously been suggested in the context of Au nanoparticles [16–18]. In our model, it arises because the effect of an applied magnetic field is to modify the coherent state and induce giant orbital paramagnetism of electrons in the coherent domains. We extended the simple theory based on coherent domains of noninteracting spinless electrons [52] to explain the anhysteretic, temperature-independent saturating paramagnetic response of agglomerates of CeO_2 nanoparticles. The response of the mesoscopic domains to an applied magnetic field is calculated in Ref. [19]. The mixing in the coherent state is modified by the static magnetic field, and the magnetic response is obtained by evaluating the expectation value of $\Sigma\mu_c.B$, where μ_c is the magnetic moment per coherent electron. The magnetic response is temperature independent, because the magnetic field mixes two states that are widely separated in energy, rather like the Van Vleck theory of temperature-independent
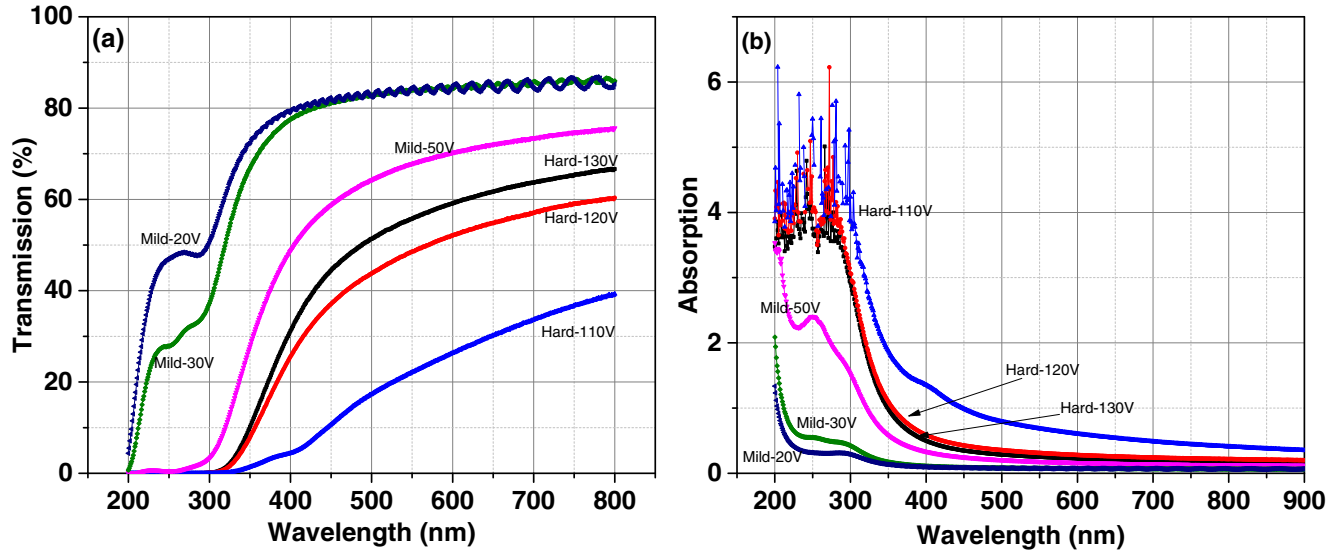
FIG. 11. (a) Transmission and (b) absorption of a set of amorphous alumina membranes including mild- and hard-anodized samples.

linear paramagnetism. Thermal excitations between them are negligible since their separation is several electron volts.

Details can be found in the supplemental information to Ref. [19], where magnetization curves are predicted to follow the theoretical expression

$$M = M_s x / \sqrt{(1 + x^2)}, \tag{3}$$

with $x = C \mu_0 H$. Fitting the magnetization curves of the alumina membranes yields values of $C = 6.0 \pm 1.1 \, \text{T}^{-1}$ for the mild samples and slightly larger values $C = 6.7 \pm 1.2 \, \text{T}^{-1}$ for the hard ones. The characteristic wavelength λ of the radiation involved is related to C in the theory by

$$\lambda = [(C/M_s)(6\hbar c \, f_c)]^{1/4}, \tag{4}$$

where f_c is taken as the volume fraction of the sample that is magnetically coherent. An upper estimate of f_c in these membranes is the alumina volume fraction $f_c = 1 - 2\pi r^2/3d^2$. For the most-magnetic mild-anodized membranes, $M_s \approx 60 \, \text{Am}^{-1}$ and $f_c \approx 0.83$; Eq. (4) yields $\lambda = 338$ nm. For the most-magnetic hard-anodized membranes, $M_s \approx 100 \, \text{Am}^{-1}$ and $f_c \approx 0.98$; and coincidentally $\lambda = 338$ nm again. It is very interesting that a comparison of the UV absorption spectra of strongly and weakly magnetic and nonmagnetic membranes exhibits absorption in the 200–300-nm range (Fig. 11). These wavelengths may be resonant with cavity modes in the pores, provided $t_m > \lambda$, or possibly with plasmoniclike modes determined by the interpore spacing. The order of magnitude of the number of electrons N in a coherent domain is $2\pi r \lambda \sigma_e$ where σ_e is the electron density associated with oxygen defects at the

pore surface. There are 18 oxygen ions per square nanometer, so a value of 1–10 electrons per square nanometer for σ_e would give $N \sim 10^5 - 10^6$.

Finally, we consider the effect of changing the direction of magnetic field. The observation is that there is no difference in the magnetic response regardless of whether the field is applied in-plane or perpendicular to the plane of the membrane. We could not reproduce the results of Sun *et al.* [25] for very brief mild anodization at 40 V in oxalic acid. The theory of the magnetism [19] is based on quantum-mechanical mixing of the ground- and excited states in the applied magnetic field, neither of which corresponds to a well-defined orbital state of the system. It follows that there is no preferred direction and no anisotropy of the paramagnetic magnetization process beyond that due to shape anisotropy, which we have seen should be negligible on account of the very small magnetization.

In summary, the model of giant orbital paramagnetism of spinless electrons in mesoscopic coherent domains is a simplification, but it gives a reasonable account of the physics of the phenomenon of d-zero magnetism of nanoporous amorphous alumina membranes.

V. CONCLUSIONS

Our experimental study establishes the existence of a saturating magnetic response in well-characterized nanoporous anodic alumina, a material with no d electrons, and a very large surface/volume ratio. The magnetism is anhysteretic and temperature independent, at least in the range 4–400 K. It arises from the open pore structure, and it is related to electrons associated with oxygen defects at the internal pore surfaces. The effect is largely destroyed by crystallization of the membranes or by a chemical treatment that modifies the surface structure of the amorphous alumina.

No model of conventional collective spin-based ferromagnetic order seems able to account for the results. In most of the magnetic samples, the saturation moments are $\leqslant 1 \, \mu_\text{B} \, \text{nm}^{-2}$, which is much too low a spin density to allow exchange coupling of the strength required for a Curie temperature that could

TABLE II. Unpaired spin densities deduced from EPR and magnetization measurements.

Voltage	Spins/kg	Density (ppm)	$m(\text{Am}^2)$	Moment density (ppm)
20	2.4×10^{19}	2.0	1.5×10^{-9}	89
70	4.6×10^{20}	39.0	70×10^{-9}	149
140	7.4×10^{20}	62.6	80×10^{-9}	307

explain the temperature independence of the magnetization. The model of saturating giant orbital paramagnetism of electrons in coherent mesoscopic domains is able to account for the magnetization curves, and it predicts optical absorption in the UV around 200–300 nm, in accordance with observations. The orbital magnetism in this spinless model is not spontaneous; it is induced by the applied field, and results from field-induced quantum-mechanical mixing of the collective ground- and excited states of the system. Hence there is no temperature dependence [19]. Spin-orbit coupling at the curved surfaces of the pores may well play a role, and it should be considered in

future, as well as the nature of the defect network at the pore surfaces that gives rise to the necessary delocalized electronic states.

[1] J. M. D. Coey, d^0 ferromagnetism, Solid State Sci. **7**, 660 (2005).

[2] J. M. D. Coey, Magnetism of dilute oxides, in *Handbook of Spin Transport and Magnetism*, edited by I Zutic and E. Y. Tsymbal (CRC, Boca Raton, FL, 2011), pp. 405–425.

[3] M. A. Garcia, E. F. Pinel, J. d. l. Venta, A. Quesada, V. Bouzas, J. F. Fernández, J. J. Romero, M. S. M. González, and J. L. Costa-Krämer, Sources of experimental errors in the observation of nanoscale magnetism, J. Appl. Phys. **105**, 013925 (2009).

[4] D. W. Abraham, M. M. Frank, and S. Guha, Absence of magnetism in hafnium oxide films, Appl. Phys. Lett. **87**, 252502 (2005).

[5] Y. Belghazi, G. Schmerber, S. Colis, J. L. Rehspringer, A. Dinia, and A. Berrada, Extrinsic origin of ferromagnetism in ZnO and $Zn_{0.9}Co_{0.1}O$ magnetic semiconductor films prepared by sol-gel technique, Appl. Phys. Lett. **89**, 122504 (2006).

[6] A. Ney, T. Kammermeier, V. Ney, K. Ollefs, and S. Ye, Limitations of measuring small magnetic signals of samples deposited on a diamagnetic substrate, J. Magn. Magn. Mater. **320**, 3341 (2008).

[7] L. M. C. Pereira, J. P. Araujo, M. J. Van Bael, K. Temst, and A. Vantomme, Practical limits for detection of ferromagnetism using highly sensitive magnetometry techniques, J. Phys. D: Appl. Phys. **44**, 215001 (2011).

[8] M. Khalid, A. Setzer, M. Ziese, P. Esquinazi, D. Spemann, A. Pöppl, and E. Goering, Ubiquity of ferromagnetic signals in common diamagnetic oxide crystals, Phys. Rev. B **81**, 214414 (2010).

[9] K. Potzger and S. Zhou, Non-DMS related ferromagnetism in transition metal doped zinc oxide, Phys. Status Solidi B **246**, 1147 (2009).

[10] B. B. Straumal, A. A. Mazilkin, S. G. Protasova, A. A. Myatiev, P. B. Straumal, G. Schütz, P. A. van Aken, E. Goering, and B. Baretzky, Magnetization study of nanograined pure and Mn-doped ZnO films: Formation of a ferromagnetic grain-boundary foam, Phys. Rev. B **79**, 205206 (2009).

[11] J. M. D. Coey, M. Venkatesan, and P. Stamenov, Surface magnetism of strontium titanate, J. Phys.: Condens. Matter **28**, 485001 (2016).

[12] M. Venkatesan, C. B. Fitzgerald, and J. M. D. Coey, Thin films: Unexpected magnetism in a dielectric oxide, Nature (London) **430**, 630 (2004).

[13] R. Jiang and Y. Zhang, Observation of ferromagnetism in highly oxygen-deficient HfO_2 films, J. Semicond. **30**, 102002 (2009).

[14] S. S. Rao, Y. F. Lee, J. T. Prater, A. I. Smirnov, and J. Narayan, Laser annealing induced ferromagnetism in $SrTiO_3$ single crystal, Appl. Phys. Lett. **105**, 042403 (2014).

[15] A. Sundaresan, R. Bhargavi, N. Rangarajan, U. Siddesh, and C. N. R. Rao, Ferromagnetism as a universal feature of nanoparticles of the otherwise nonmagnetic oxides, Phys. Rev. B **74**, 161306(R) (2006).

[16] A. Hernando, P. Crespo, M. A. García, J. M. D. Coey, A. Ayuela, and P. M. Echenique, Revisiting magnetism of capped Au and ZnO nanoparticles: Surface band structure and atomic orbital with giant magnetic moment, Phys. Status Solidi B **248**, 2352 (2011).

[17] G. L. Nealon, B. Donnio, R. Greget, J.-P. Kappler, E. Terazzi, and J.-L. Gallani, Magnetism in gold nanoparticles, Nanoscale **4**, 5244 (2012).

[18] R. Gréget, G. L. Nealon, B. Vileno, P. Turek, C. Mény, F. Ott, A. Derory, E. Voirin, E. Rivière, A. Rogalev, F. Wilhelm, L. Joly, W. Knafo, G. Ballon, E. Terazzi, J.-P. Kappler, B. Donnio, and J.-L. Gallani, Magnetic properties of gold nanoparticles: A room-temperature quantum effect, Chem. Phys. Chem. **13**, 3092 (2012).

[19] J. M. D. Coey, K. Ackland, M. Venkatesan, and S. Sen, Collective magnetic response of CeO_2 nanoparticles, Nat. Phys. **12**, 694 (2016).

[20] K. Ackland and J. M. D. Coey, Room temperature magnetism in CeO_2 – A review, Phys. Rep. (2018), doi:10.1016/j.physrep.2018.04.002.

[21] A. Ohtomo and H. Y. Hwang, A high-mobility electron gas at the $LaAlO_3/SrTiO_3$ heterointerface, Nature (London) **427**, 423 (2004).

[22] G. Herranz, M. Basletic, M. Bibes, C. Carretero, E. Tafra, E. Jacquet, K. Bouzehouane, C. Deranlot, A. Hamzic, J. M. Broto, A. Barthelemy, and A. Fert, High Mobility in $LaAlO_3/SrTiO_3$ Heterostructures: Origin, Dimensionality, and Perspectives, Phys. Rev. Lett. **98**, 216803 (2007).

[23] Z. Q. Liu, W. M. Lü, S. L. Lim, X. P. Qiu, N. N. Bao, M. Motapothula, J. B. Yi, M. Yang, S. Dhar, T. Venkatesan, and Ariando, Reversible room-temperature ferromagnetism in Nb-doped $SrTiO_3$ single crystals, Phys. Rev. B **87**, 220405(R) (2013).

[24] K. Potzger, J. Osten, A. A. Levin, A. Shalimov, G. Talut, H. Reuther, S. Arpaci, D. Bürger, H. Schmidt, T. Nestler, and D. C. Meyer, Defect-induced ferromagnetism in crystalline $SrTiO_3$, J. Magn. Magn. Mater. **323**, 1551 (2011).

[25] H. Y. Sun, H. M. Zhang, X. Hou, L. H. Liu, T. S. Wu, and S. M. Yang, Significant room temperature ferromagnetism in PAA thin films, J. Mater. Chem. C **1**, 3569 (2013).

[26] T. S. Wu, H. Y. Sun, X. Hou, L. H. Liu, H. M. Zhang, and J. J. Zhang, Significant room-temperature ferromagnetism in porous TiO_2 thin films, Microporous Mesoporous Mater. **190**, 63 (2014).

[27] X. Hou, H. Sun, L. Liu, X. Jia, and H. Liu, Unexpected large room-temperature ferromagnetism in porous Cu_2O thin films, J. Magn. Magn. Mater. **382**, 20 (2015).

[28] L. Q. Qi, H. Y. Liu, H. Y. Sun, L. H. Liu, and R. S. Han, Electric field control of magnetization in Cu_2O/porous anodic alumina hybrid structures at room temperature, Appl. Phys. Lett. **108**, 142402 (2016).

[29] H. Masuda and K. Fukuda, Ordered metal nanohole arrays made by a 2-step replication of honeycomb structures of anodic alumina, Science **268**, 1466 (1995).

[30] W. Lee, R. Ji, U. Gosele, and K. Nielsch, Fast fabrication of long-range ordered porous alumina membranes by hard anodization, Nat. Mater. **5**, 741 (2006).

[31] S. Davis and G. Gutierrez, Structural, elastic, vibrational and electronic properties of amorphous Al_2O_3 from *ab initio* calculations, J. Phys.: Condens. Matter **23**, 495401 (2011).

[32] A. S. Esmaeily, S. Mills, and J. M. D. Coey, Exceptional room-temperature plasticity in amorphous alumina nanotubes fabricated by magnetic hard anodization, Nanoscale **9**, 5205 (2017).

[33] J. M. D. Coey, *Magnetism and Magnetic Materials* (Cambridge University Press, Cambridge, England, 2010).

[34] M. Ata, Y. Liu, and I. Zhitomirsky, A review of new methods of surface chemical modification, dispersion and electrophoretic deposition of metal oxide particles, RSC Adv. **4**, 22716 (2014).

[35] X. Sun, F. Xu, Z. Li, and W. Zhang, Photoluminescence properties of anodic alumina membranes with ordered nanopore arrays, J. Lumin. **121**, 588 (2006).

[36] M. Venkatesan, P. Kavle, S. B. Porter, K. Ackland, and J. M. D. Coey, Magnetic analysis of polar and nonpolar oxide substrates, IEEE Trans. Magn. **50**, 1 (2014).

[37] B. Abad, J. Maiz, and M. Martin-Gonzalez, Rules to Determine thermal conductivity and density of anodic aluminum oxide (AAO) membranes, J. Phys. Chem. C **120**, 5361 (2016).

[38] J. M. D. Coey, P. Stamenov, R. Gunning, M. Venkatesan, and K. Paul, Ferromagnetism in defect-ridden oxides and related materials, New J. Phys. **12**, 053025 (2010).

[39] T. Tietze, P. Audehm, Y. C. Chen, G. Schütz, B. B. Straumal, S. G. Protasova, A. A. Mazilkin, P. B. Straumal, T. Prokscha, H. Luetkens, Z. Salman, A. Suter, B. Baretzky, K. Fink, W. Wenzel, D. Danilov, and E. Goering, Interfacial dominated ferromagnetism in nanograined ZnO: A μSR and DFT study, Sci. Rep. **5**, 8871 (2015).

[40] B. B. Straumal, A. A. Mazilkin, S. G. Protasova, A. A. Myatiev, P. B. Straumal, E. Goering, and B. Baretzky, Amorphous grain boundary layers in the ferromagnetic nanograined ZnO films, Thin Solid Films **520**, 1192 (2011).

[41] R. Podila, W. Queen, A. Nath, J. T. Arantes, A. L. Schoenhalz, A. Fazzio, G. M. Dalpian, J. He, S. J. Hwu, M. J. Skove, and A. M. Rao, Origin of FM ordering in pristine micro- and nanostructured ZnO, Nano Lett. **10**, 1383 (2010).

[42] G. Gopal Khan, A. K. Singh, and K. Mandal, Structure dependent photoluminescence of nanoporous amorphous anodic aluminium oxide membranes: Role of F+ center defects, J. Lumin. **134**, 772 (2013).

[43] H. Momida, S. Nigo, G. Kido, and T. Ohno, Effect of vacancy-type oxygen deficiency on electronic structure in amorphous alumina, Appl. Phys. Lett. **98**, 042102 (2011).

[44] F. Esch, S. Fabris, L. Zhou, T. Montini, C. Africh, P. Fornasiero, G. Comelli, and R. Rosei, Electron localization determines defect formation on ceria substrates, Science **309**, 752 (2005).

[45] Y. Du, W. L. Cai, C. M. Mo, J. Chen, L. D. Zhang, and X. G. Zhu, Preparation and photoluminescence of alumina membranes with ordered pore arrays, Appl. Phys. Lett. **74**, 2951 (1999).

[46] Y. Li, G. Li, G. Meng, L. Zhang, and F. Phillipp, Photoluminescence and optical absorption caused by the F^+ centres in anodic alumina membranes, J. Phys.: Condens. Matter **13**, 2691 (2001).

[47] G. H. Li, Y. Zhang, Y. C. Wu, and L. D. Zhang, Photoluminescence of anodic alumina membranes: Pore size dependence, Appl. Phys. A **81**, 627 (2005).

[48] J. Chen, C. Huang, C. Chao, and T. Chen, The investigation of photoluminescence centers in porous alumina membranes, Appl. Phys. A **84**, 297 (2006).

[49] A. Nourmohammadi, S. J. Asadabadi, M. H. Yousefi, and M. Ghasemzadeh, Photoluminescence emission of nanoporous anodic aluminum oxide films prepared in phosphoric acid, Nanoscale Res. Lett. **7**, 689 (2012).

[50] G.-D. Li, Q. Wang, B.-X. Deng, and Y.-J. Zhang, Origin of nanopore alumina film photoluminescence: Three kinds of defect centers, Acta Phys. Sin. **63**, 247802 (2014).

[51] D. O. Ilin, A. S. Vokhmintsev, and I. A. Weinstein, Luminescence characteristics of nanoporous anodic alumina annealed at different temperatures, AIP Conf. Proc. **1767**, 020028 (2016).

[52] S. Sen, K. S. Gupta, and J. M. D. Coey, Mesoscopic structure formation in condensed matter due to vacuum fluctuations, Phys. Rev. B **92**, 155115 (2015).

[53] A. Canaguier-Durand, E. Devaux, J. George, Y. Pang, J. A. Hutchison, T. Schwartz, C. Genet, N. Wilhelms, J.-M. Lehn, and T. W. Ebbesen, Thermodynamics of molecules strongly coupled to the vacuum field, Angew. Chem., Int. Ed. **52**, 10533 (2013).

[54] A. Shalabney, J. George, J. Hutchison, G. Pupillo, C. Genet, and T. W. Ebbesen, Coherent coupling of molecular resonators with a microcavity mode, Nat. Commun. **6**, 5981 (2015).

[55] J. A. Hutchison, A. Liscio, T. Schwartz, A. Canaguier-Durand, C. Genet, V. Palermo, P. Samorì, and T. W. Ebbesen, Tuning the work-function via strong coupling, Adv. Mater. **25**, 2481 (2013).

[56] E. Orgiu, J. George, J. A. Hutchison, E. Devaux, J. F. Dayen, B. Doudin, F. Stellacci, C. Genet, J. Schachenmayer, C. Genes, G. Pupillo, P. Samori, and T. W. Ebbesen, Conductivity in organic semiconductors hybridized with the vacuum field, Nat. Mater. **14**, 1123 (2015).

[57] T. Chervy, J. Xu, Y. Duan, C. Wang, L. Mager, M. Frerejean, J. A. W. Münninghoff, P. Tinnemans, J. A. Hutchison, C. Genet, A. E. Rowan, T. Rasing, and T. W. Ebbesen, High-efficiency second-harmonic generation from hybrid light-matter states, Nano Lett. **16**, 7352 (2016).

[58] T. W. Ebbesen, Hybrid light–matter states in a molecular and material science perspective, Acc. Chem. Res. **49**, 2403 (2016).